

DesignCon 2008

Analysis of Crosstalk Effects on Jitter in Transceivers

Daniel Chow, Altera Corporation
dchow@altera.com

Abstract

As data rates increase, crosstalk becomes an increasingly important issue. Crosstalk aggressors can attack both amplitude and timing characteristics of the victim signal. The effects of crosstalk on the jitter of a victim signal are not well understood because crosstalk does not fit neatly into the standard definitions of jitter components. As a result, most commercially available jitter analyzers misinterpret crosstalk. We investigate the effects of various types of crosstalk aggressors on a victim signal in a transceiver, with particular emphasis on jitter. We also demonstrate cases where crosstalk is misinterpreted as random jitter (RJ), periodic jitter (PJ), or intersymbol interference (ISI).

Author Biography

Dr. Daniel Chow is a senior member of technical staff in the characterization group at Altera Corporation. His responsibilities include testing and validation of high-speed components. Specifically, he is responsible for developing Altera's knowledge base on jitter measurement issues. Dr. Chow received his Ph.D. from the University of California, Davis.

Background and Motivation

In the field of high-speed data communications, crosstalk becomes an increasingly important issue as data rates increase. Crosstalk can occur anywhere in the system, such as the silicon die, package, or printed circuit board. Crosstalk can affect the voltage and/or timing characteristics of the victim signal, depending on the nature of the coupling between the aggressor and victim. The effects of crosstalk on the victim's voltage are straightforward [1]. However, the effects of crosstalk on the victim's timing jitter are less understood.

The theories and practices of high-speed timing jitter are well established. Quantities such as random jitter (RJ), periodic jitter (PJ), data-dependent jitter (DDJ), deterministic jitter (DJ), and total jitter (TJ), are well-understood and widely accepted [2]. However, only minimal consideration has been given to crosstalk phenomena in the form of bounded, uncorrelated jitter (BUJ) [3,4].

Since jitter caused by crosstalk is not clearly addressed by the standard definitions of jitter components, most commercially available jitter analyzers are unable to measure it and may misinterpret it as one of the common components of jitter, such as RJ, PJ, or DDJ. In particular, if the victim's RJ rms value is contaminated, the estimated total jitter is even more severely impacted. We examine real-life situations for each of these cases. This knowledge will help engineers diagnose crosstalk issues by recognizing its effects.

What is Crosstalk?

Crosstalk, and noise coupling in general, is defined as an interference between two signals in such a way that one signal creates an undesired effect in another signal [5]. Within this broad definition, we can define two categories of crosstalk. In one category, the aggressor signal primarily affects the voltage characteristics of the victim signal. In the other category, the aggressor signal primarily affects the timing characteristics of the victim signal.

For an aggressor attacking a victim's voltage, the coupling mechanisms are generally inductive and/or capacitive between the two signals [5]. Typically, this is caused by two signal traces being in close proximity to each other. Naturally, any impact on the voltage of the victim will have a secondary effect on the timing of the victim due to slopes of the transition edges. This type of coupling has been explored extensively and is generally well-understood [1].

For an aggressor attacking a victim's timing, the coupling is usually between the aggressor and the victim signal's power supply or clock. The result is that the aggressor corrupts the timing of the victim signal. This type of coupling is often discussed, but not always well understood.

In addition to the coupling mechanism, the effects of crosstalk strongly depend on the relationships between various properties of the aggressor and victim signals such as data rate, phase, and data pattern.

Signal Spectra vs. Jitter Spectra

When considering issues in signal integrity and jitter, it is important to clarify concepts such as power spectrum and jitter spectrum. Figure 1 shows plots for a voltage waveform, power spectrum, jitter time interval error (TIE) [6], and jitter spectrum.

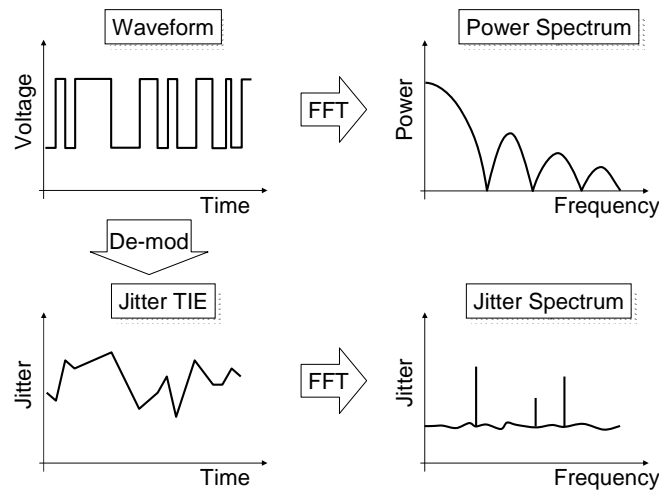


Figure 1: Relationships between waveform, waveform spectrum, jitter, and jitter spectrum.

The voltage waveform is the signal seen in a typical oscilloscope with time on the x-axis and voltage on the y-axis. This is how the signal is commonly visualized. The power spectrum is the Fourier transform (or equivalent) of the waveform with frequency on the x-axis and typically power on the y-axis.

The jitter TIEs are the timing errors of the data obtained by demodulation from the waveform. The TIE shows the fluctuation of jitter as a function of time. Because jitter is expressed in units of time, the TIE plot has units of time in both axes. The jitter spectrum is the Fourier transform (or equivalent) of the jitter TIE with frequency on the x-axis and time on the y-axis.

In crosstalk cases where an aggressor attacks a victim's voltage, the aggressor's waveform is coupled to the victim's waveform. Equivalently, the aggressor's power spectrum is coupled to the victim's power spectrum. However, for an aggressor attacking a victim's timing, the aggressor's waveform is coupled to the victim's jitter TIE. Equivalently, the aggressor's power spectrum is coupled to the victim's jitter spectrum. These differences are crucial to understanding the effects of crosstalk.

Spectra for Common Data Waveforms

It is intuitive to think about noise coupling between the aggressor and victim in the time domain. But in order to have a full understanding of crosstalk, significant consideration must be given to the frequency spectra of the signals. The spectra of data waveforms are often non-intuitive, especially when coupling mechanisms are considered. We review the

fundamentals of frequency spectra for common signals, then builds up an understanding of spectra for more complicated waveforms.

Waveform Spectra

For a single, non-repeating square pulse of width T_0 and instantaneous rise and fall times, the corresponding power spectrum is the familiar continuum of frequencies represented by a rectified sinc ($\sin(x)/x$) function (Figure 2). We define a fundamental frequency $f_0 = 1/T_0$. This spectrum has zeros at multiples of f_0 , and peaks at odd multiples of $f_0/2$. Since the square pulse serves as the basic building block for waveforms of binary digital data, the corresponding spectrum is important in the understanding of power spectra for data waveforms.

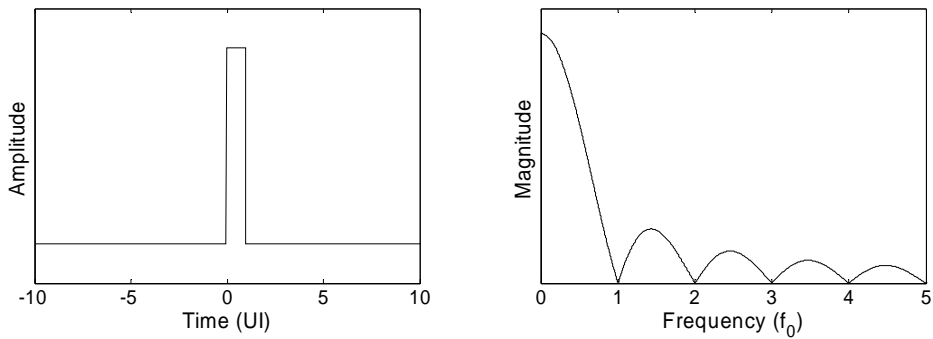


Figure 2: Simulated waveform and spectrum for a square pulse.

Figure 3 shows the measured continuous spectrum of a square pulse. The measurement closely matches the expectation. Note that the magnitude in Figure 2 is in a linear scale while the magnitude in Figure 3 is in a logarithmic scale.

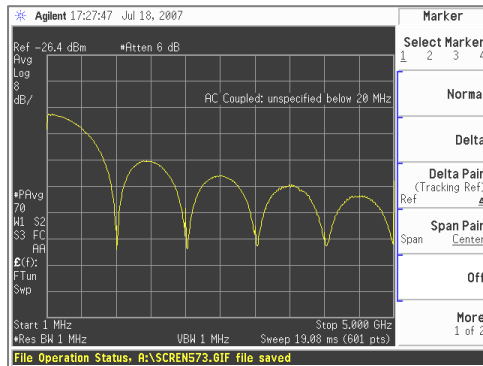


Figure 3: Measured spectrum for a square pulse.

For a square wave with pulse width of T_0 and period of $2T_0$, also with instantaneous rise and fall times (Figure 4), the corresponding spectrum is also familiar, consisting of discrete spectral lines at odd harmonics of the fundamental frequency $f_0/2$. The frequencies and relative amplitudes of the spikes of the square wave match the peaks of the side lobes of the square pulse's spectrum due to the same pulse widths in both signals.

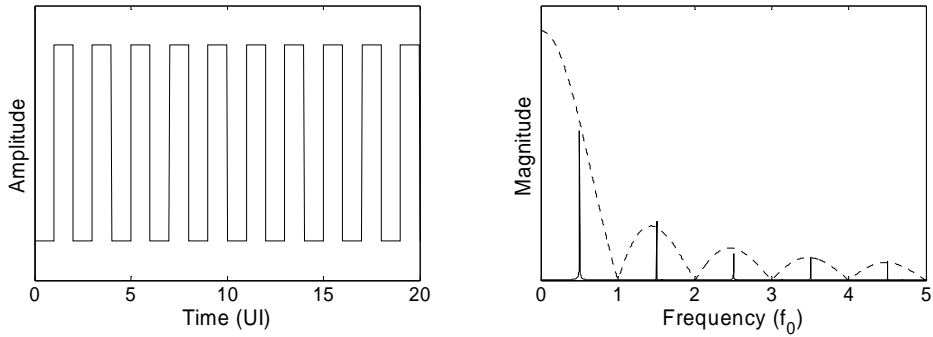


Figure 4: Simulated waveform and spectrum for a square wave. The dotted line is a rectified sinc function.

Figure 5 shows the measured discrete spectrum for a square wave. The measurement closely matches the expectation. However, Figure 5 shows small artifacts at the even harmonics and the background noise, suggesting that the laboratory signal source did not produce an ideal square wave.

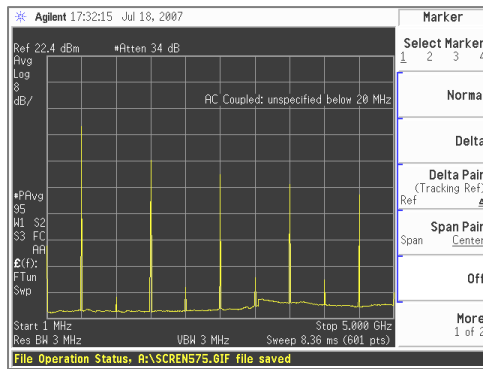


Figure 5: Measured spectrum for a square wave.

Figure 6 shows the waveform and spectra for a repeating short data pattern (k28.5, 20 bits in length) with a unit interval (UI) of T_0 and instantaneous rise and fall times. While the waveform is easily recognizable, the corresponding spectrum is probably unfamiliar to most. The spectrum consists of many discrete lines whose relative amplitudes are bounded by a rectified sinc envelope.

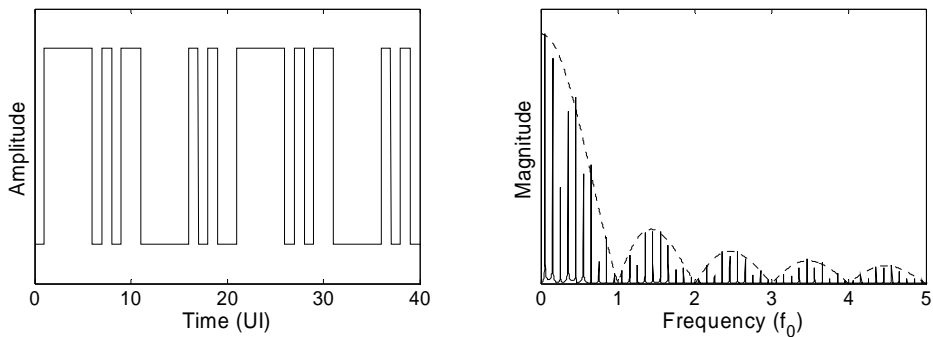


Figure 6: Simulated waveform and spectrum for a k28.5 data pattern. The dotted line is a rectified sinc function.

This data pattern repeats every $20T_0$. The pattern repeat frequency is defined as $f_{\text{Pat}} = 1/(20T_0) = f_0/20$. The entire data pattern can be thought of as an arbitrary waveform that repeats every $20T_0$. A Fourier series of this arbitrary waveform consists of the fundamental frequency f_{Pat} and harmonics.

Figure 6 shows that the fundamental frequency of these discrete lines is $f_0/20$, which agrees with the above analysis. However, it is also notable that the spectrum has only odd harmonics of f_{Pat} because the k28.5 pattern has odd symmetry.

Figure 7 shows the measured spectrum for a k28.5 pattern. Again, the measurement closely matches the expectation from the simulation, including the presence of only the odd harmonics of f_{Pat} .

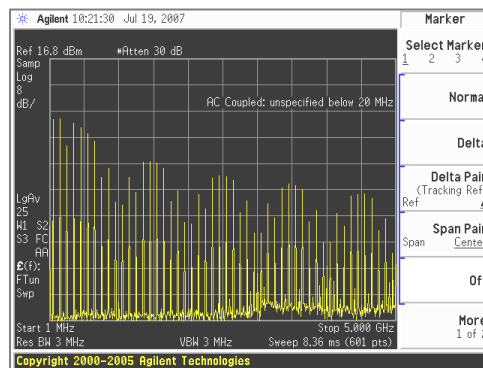


Figure 7: Measured spectrum for a short data pattern (k28.5).

Figure 8 shows the waveform and spectrum for a longer data pattern (PRBS 2^7-1 , 127 bits in length). This spectrum also consists of numerous discrete lines bounded by a rectified sinc envelope.

For this pattern, $f_{\text{Pat}} = f_0/127$. As with the previous case, the discrete spectrum has a fundamental frequency of f_{Pat} and harmonics. All harmonics are present because PRBS 2^7-1 has no symmetry.

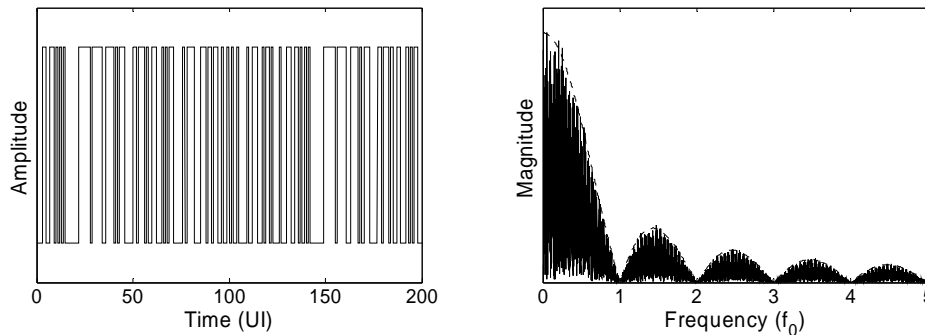


Figure 8: Simulated waveform and spectrum for a PRBS 2^7-1 data pattern. The dotted line is a rectified sinc function.

Figure 9 shows the measured spectrum for a PRBS 2^7-1 pattern. The measurement also closely matches the expectation from the simulation, showing a dense set of discrete lines at multiples of f_{pat} bounded by a rectified sinc function.

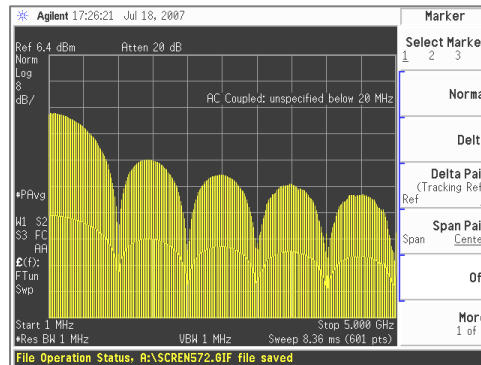


Figure 9: Measured spectrum for a longer data pattern (PRBS 2^7-1).

Several conclusions about the spectra of data patterns can be drawn from these simulations and laboratory demonstrations. The spectral profile is bounded by an envelope given by the spectrum of the basic unit of the waveform. In this case, the basic unit is a square pulse and the corresponding spectrum is a rectified sinc function.

Repeating data patterns have spectra that consist of discrete lines. The spacing of the discrete lines is inversely proportional to the pattern length. Short patterns have wide line spacing and vice versa. For an infinitely long, non-repeating pattern, the spectral line spacing is infinitesimal, effectively making the spectrum continuous.

It is important to note that, for both simulation and measurement, the resolution bandwidth window of the spectrum can alter the appearance of the spectrum. If the resolution bandwidth is greater than the spacing of the discrete lines, the discrete lines would not be resolved and the spectrum would appear to be continuous. In order to resolve the discrete lines, the resolution bandwidth of the spectrum must be smaller than the line spacing.

Coupling Spectra (Delta Functions)

For capacitive or inductive coupling, the aggressors couple to the victims by $L(dI/dt)$ or $C(dV/dt)$, respectively. Both mechanisms depend on the time derivative of the aggressor waveform. For an ideal signal with zero rise and fall times, the time derivative of the waveform results in positive and negative Dirac delta functions, respectively.

Thus, the aggressor's coupling spectra are different from the waveform spectra shown in Section 0. For the single, non-repeating square pulse shown in Figure 2, the time derivative of the waveform and corresponding spectrum is shown in Figure 10. The derivative of the square wave consists of one positive delta function and one negative delta function, corresponding to the rising and falling edges, respectively.

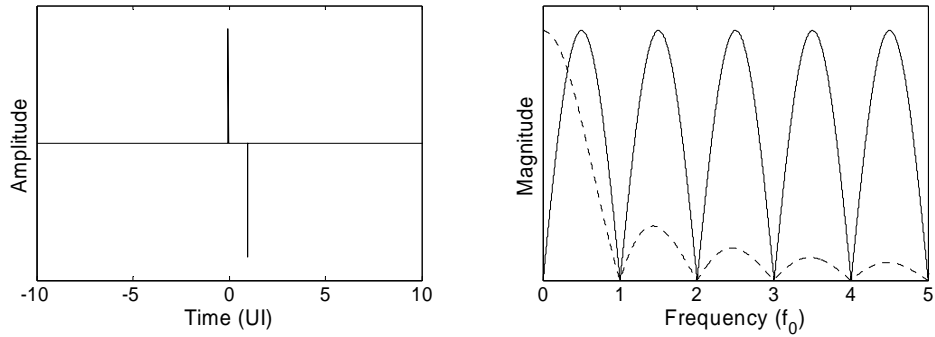


Figure 10: Simulated waveform and spectrum for the derivative of a square pulse. The dotted line is a rectified sine function.

There are two significant differences between the spectrum of the square pulse and its derivative. First, the spectrum of the two delta functions is a rectified sine wave with zeros at harmonics of f_0 . The spectrum is infinitely broad and does not attenuate with increasing frequency. Secondly, the spectrum has a zero at the origin, leading to a lack of low frequency power. In contrast, the square wave spectrum has most of its power at low frequencies, even at dc. These dramatic differences must be considered when working with noise coupling issues.

Figure 11 shows the time derivative of a square wave and the corresponding spectrum. Similar to Figure 4, there are discrete lines at odd harmonics of $f_0/2$ with amplitudes bounded by a rectified sine function.

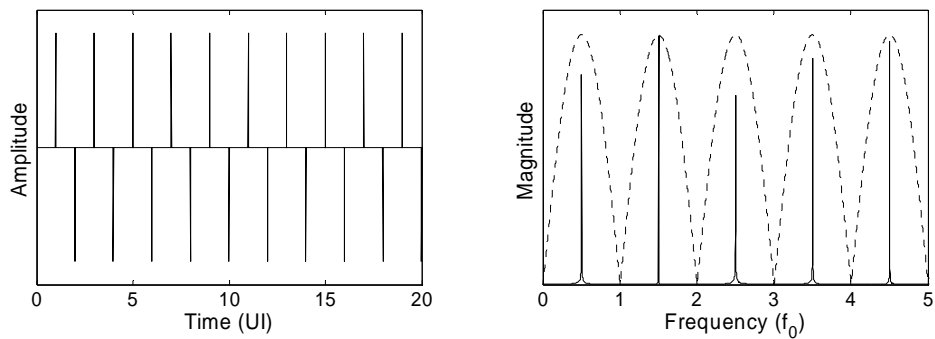


Figure 11: Simulated waveform and spectrum for the derivative of a square wave. The dotted line is a rectified sine function.

Figure 12 shows the time derivative of a short data pattern (k28.5) and the corresponding spectrum. The location of the discrete lines matches those of the original waveform shown in Figure 6. The amplitudes are bounded by a rectified sine envelope, just as in Figure 11.

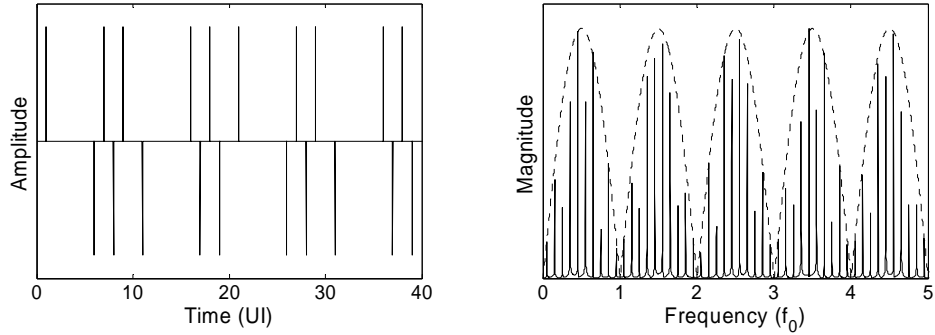


Figure 12: Simulated waveform and spectrum for the derivative of a k28.5 data pattern. The dotted line is a rectified sine function.

Figure 13 shows the time derivative and corresponding waveform for a longer data pattern (PRBS 2^7-1). Again, the location of the discrete lines and amplitude envelope match the corresponding cases shown in Figure 8 and Figure 10, respectively.

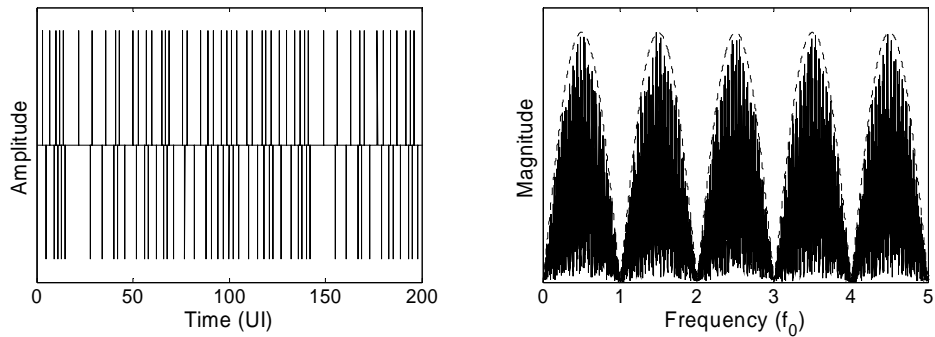


Figure 13: Simulated waveform and spectrum for the derivative of a PRBS 2^7-1 data pattern. The dotted line is a rectified sine function.

These simulations further confirm that the spectral profile is bounded by an envelope that is given by the spectrum of the basic unit of the waveform. In this case, the basic unit is a pair of alternating delta functions whose spectrum is a rectified sine function. The locations of the discrete spectral lines depend on the pattern length and are consistent with the respective spectra of the original waveforms.

Coupling Spectra (Exponential Functions)

The delta function treatment in Section 0 assumes no resistance in the capacitive or inductive couplings. In reality, any Ohmic resistance alters the coupling waveform to become exponential decays with time a constant of $1/RC$ or L/R .

We again examine the various waveforms with exponential decays corresponding to the rising and falling edges, starting with the square pulse (Figure 14). The corresponding spectrum again differs from the previous spectra, but retains familiar elements.

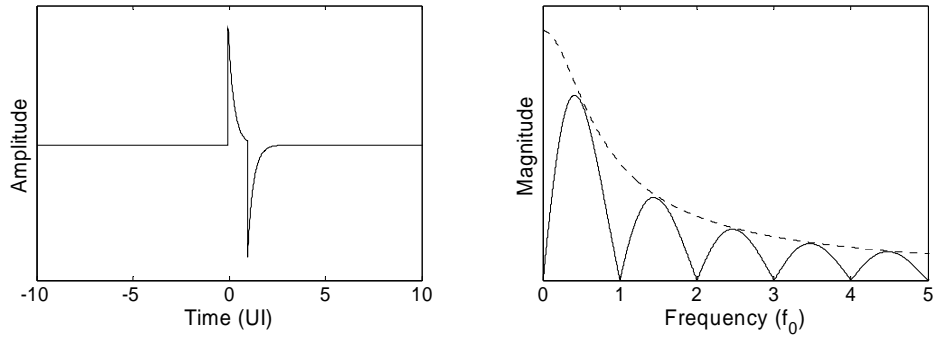


Figure 14: Simulated waveform and spectrum for the exponential response of a square pulse. The dotted line is a Lorentzian function.

The spectrum consists of lobes with peaks at odd multiples of $f_0/2$ and zeros at multiples of f_0 . This is similar to the rectified sine function due to sharp rising and falling edges. The amplitudes of the lobes are bounded by a Lorentzian function [7], which is the spectrum of an exponential decay.

Figure 15 shows the exponential response of a square wave. As with other variations of the square wave, the spectrum consists of discrete lines at odd multiples of $f_0/2$. The amplitudes of the spectral lines are bounded by a Lorentzian envelope.

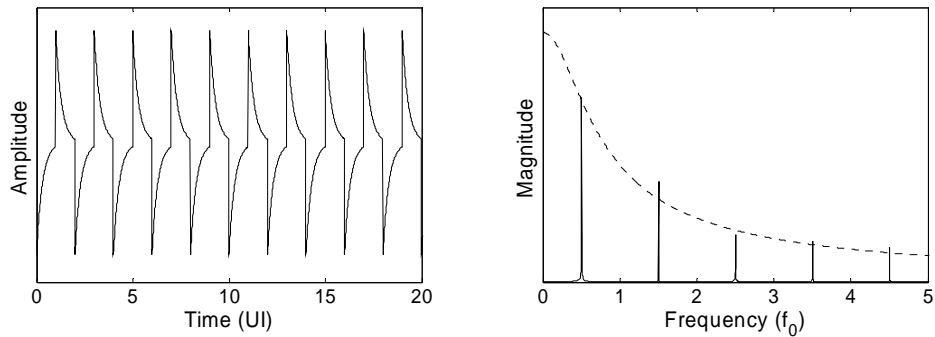


Figure 15: Simulated waveform and spectrum for the exponential response of a square wave. The dotted line is a Lorentzian function.

Figure 16 shows the exponential response of a k28.5 data pattern. The discrete lines are located the same as other waveform variations of the k28.5 pattern. The amplitudes of the spectral lines are bounded by a rectified sine function attenuated by a Lorentzian.

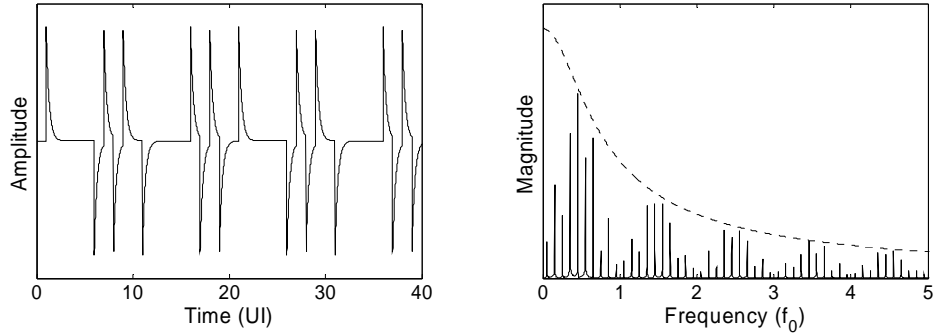


Figure 16: Simulated waveform and spectrum for the exponential response of a k28.5 data pattern. The dotted line is a Lorentzian function.

Figure 17 shows the exponential response of a PRBS 2^7-1 data pattern. The discrete lines are located the same as other waveform variations of the PRBS 2^7-1 pattern. The amplitudes of the spectral lines follow the expected envelope.

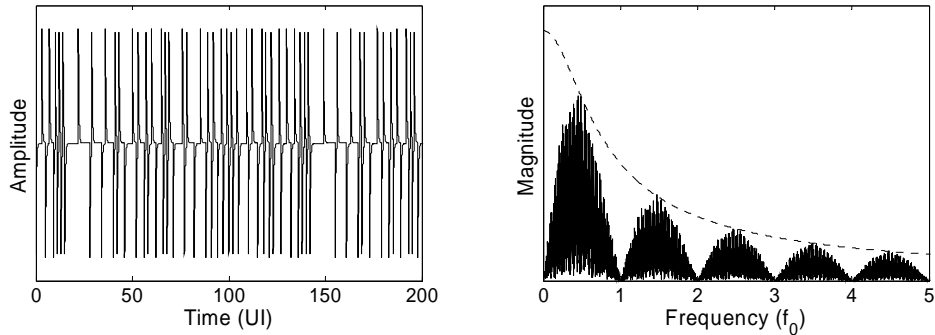


Figure 17: Simulated waveform and spectrum for the exponential response of a PRBS 2^7-1 data pattern. The dotted line is a Lorentzian function.

Again, these simulations confirm our understanding of spectra of various waveforms. The power spectrum is strongly dependent on the shape of the basic unit of the waveform and the data pattern. The changes in the waveform shape can come from the coupling mechanism and its parameters. This knowledge helps engineers recognize the different types of aggressor spectra for different types of noise coupling.

Crosstalk Affecting Jitter in a Transceiver

We demonstrate the effects of crosstalk on jitter by performing experiments on a transceiver test chip with a known degradation such that the power supply of the transmit buffers (Tx) was coupled to the power supply of the transmitter phase-locked loop (PLL), shown in Figure 18. In this test chip, toggling activity in the Tx causes the instantaneous power sagging of the V_{cc} , which in turn corrupts the power integrity of the PLL, causing timing errors in all channels. Effectively, this setup allows the aggressors' voltage signal to attack the victim's clock source.

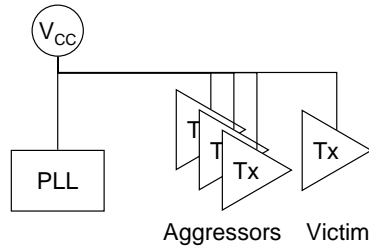


Figure 18: Schematic for shared power supply between the PLL and transmitters in a test chip.

There are numerous possible combinations of the relationship between the aggressor and the victim. This experiment focuses on varying only the data pattern. Despite its apparent simplicity, this experiment is sufficient to show that different aggressor data patterns can be misinterpreted as RJ, PJ, or DDJ by common jitter analyzers.

Setup

The transmitters were operated in a quad mode such that the signals in all four channels are frequency-locked and in phase with each other. All channels were transmitting at 2.5 Gbps. The victim channel had an output differential voltage $V_{OD} = 800\text{mV}$. The three aggressors had $V_{OD} = 1400\text{mV}$ plus maximum pre-emphasis settings. This setup maximized the impact of the aggressors, providing a clear demonstration of the effects of crosstalk on jitter. The victim signal was measured by two conventional jitter analyzers: an equivalent-time sampling oscilloscope (a.k.a., “sampling scope”) and a real-time sampling oscilloscope (a.k.a., “real-time scope”). The sampling scope has an analog bandwidth of 18 GHz. The real-time scope has an analog bandwidth of 6 GHz and a sampling rate of 20 GSamples/s.

Baseline Measurement

The victim channel transmitted a PRBS $2^{10}-1$ data pattern. With the aggressors disabled, the victim’s output jitter was measured. The results are shown in Table 1. For simplicity, only RJ, PJ, DDJ, and TJ at 10^{-12} bit error rate (BER) are shown. RJ was reported as an rms value. PJ for the sampling scope was reported as a delta-to-delta ($\delta-\delta$) value due to the dual-Dirac delta model for jitter separation [8]. All other jitter values are peak-to-peak.

Jitter	Sampling Scope	Real-Time Scope
RJ	3.27 ps	3.05 ps
PJ	11.5 ps ($\delta-\delta$)	3.08 ps (pk-pk)
DDJ	10.2 ps	16.6 ps
TJ	61.6 ps	62.58 ps

Table 1: Comparison of jitter values for baseline measurement.

In addition to the differences in hardware, the oscilloscopes also have very different methodologies for jitter separation and estimation. For the sampling scope’s methodology, RJ is found by measuring and integrating the jitter spectral baseline. PJ is found by measuring the uncorrelated jitter histogram and compensating for the RJ contribution. DDJ is found by isolating correlated jitter from uncorrelated jitter

histograms through mean values. TJ is found by extrapolation of the dual-Dirac model [8].

For the real-time scope's methodology, RJ is found by Q-scale fitting. PJ is found by isolating spectral lines in a jitter spectrum, DDJ is found by isolating correlated jitter from uncorrelated jitter histogram through mean values. TJ is found by extrapolation of the Q-scale [8].

Despite the two different sets of methodologies for the scopes, the data show a good correlation for RJ and TJ, which are the critical components of jitter. PJ values differ due to methodology. DDJ values differ due to analog bandwidths.

PRBS 2^7-1 Aggressors

We enabled the all three aggressor channels and configured them to transmit PRBS 2^7-1 data patterns. The aggressors' patterns were shorter than the victim's PRBS $2^{10}-1$ pattern. Table 2 shows the results. Compared with Table 1, PJ was increased significantly for both scopes: a factor of two for the sampling scope and a factor of six for the real-time scope. For both scopes, because PJ was affected, TJ was similarly affected.

Jitter	Sampling Scope	Real-Time Scope
RJ	3.6 ps	3.64 ps
PJ	24.4 ps ($\bar{\delta}-\bar{\delta}$)	19.3 ps (pk-pk)
DDJ	10.1 ps	16.6 ps
TJ	80.5 ps	87.1 ps

Table 2: Comparison of jitter values for PRBS 2^7-1 aggressor pattern.

Each scope's measurement methodology explains why PRBS 2^7-1 aggressors were misinterpreted as PJ instead of any other jitter component. For the real-time scope, PJ was found by analyzing jitter spectral lines. Since the aggressors appeared as many discrete spectral lines, the scope methodology misinterpreted these lines as PJ. RJ was consistent because the aggressors did not corrupt the Q-scale at low BER due to its relatively short length. DDJ was also uncorrupted, as the methodology isolated only the correlated jitter.

For the sampling scope, RJ was found by integration of the jitter spectral baseline. The jitter spectrum was corrupted by the aggressors' spectrum with many discrete lines, but they were excluded in the baseline integration, allowing RJ to remain consistent. The aggressors also corrupted the uncorrelated jitter histogram. Since RJ is uncorrupted, the excess jitter was attributed to PJ by the scope methodology. DDJ remains uncorrupted, as the methodology isolated only the correlated jitter.

PRBS $2^{10}-1$ Aggressors

We repeated this experiment with a different aggressor pattern, PRBS $2^{10}-1$. The aggressors' data pattern was synchronous to the victim's data pattern. The results are shown in Table 3. Because the aggressors' pattern was correlated to the victim's pattern, both scopes misinterpreted the crosstalk as DDJ in the victim signal. The sampling scope saw a three-fold increase and the real-time scope saw a two-fold increase in DDJ.

Jitter	Sampling Scope	Real-Time Scope
RJ	3.29 ps	3.45 ps
PJ	12.3 ps ($\bar{\delta}$ - $\bar{\delta}$)	4.41 ps (pk-pk)
DDJ	28.2 ps	30.7 ps
TJ	77.3 ps	98.7 ps

Table 3: Comparison of jitter values for PRBS $2^{10}-1$ aggressor pattern.

For the sampling scope, RJ was still consistent because the aggressors' discrete spectral lines did not corrupt the jitter spectrum's baseline. PJ was also consistent because the aggressors did not corrupt the uncorrelated jitter histogram.

For the real-time scope, RJ was similarly consistent because the aggressors could not corrupt the Q-scale at low BER due to its relatively short length. PJ was consistent because spectral lines corresponding to harmonics of f_{pat} were ignored, as they were considered correlated jitter.

Thus, for both scopes, the crosstalk could only appear as DDJ because of their common methodology. Again, TJ was affected by the apparent increase of DDJ.

PRBS $2^{31}-1$ Aggressors

For the final experiment, the aggressors transmitted a PRBS $2^{31}-1$ data pattern. The results are shown in Table 4. For this case, the crosstalk appeared as an increase in RJ. TJ was inflated disproportionately because TJ at $BER = 10^{-12}$ roughly scales as $14RJ$ [8].

Jitter	Sampling Scope	Real-Time Scope
RJ	6.36 ps	5.34 ps
PJ	11.3 ps ($\bar{\delta}$ - $\bar{\delta}$)	4.13 ps (pk-pk)
DDJ	9.9 ps	16.8 ps
TJ	98.7 ps	96.0 ps

Table 4: Comparison of jitter values for PRBS $2^{31}-1$ aggressor pattern.

As with the other cases, an examination of the scopes' jitter separation methodologies explains the appearance of crosstalk as RJ. For the sampling scope, the aggressors corrupted the jitter spectrum with numerous spectral lines. Unlike the previous two aggressor patterns, the spacing of these spectral lines was extremely small. The length of the PRBS $2^{31}-1$ pattern is longer than 2.1 billion bits. For the aggressor data rate of 2.5 Gbps, the pattern repeat frequency f_{pat} is approximately 0.85 Hz. This line spacing is far below the spectral resolution of this instrument, causing the aggressor spectrum to appear as a broadband baseline noise. Thus, the PRBS $2^{31}-1$ aggressors corrupted RJ in the sampling scope.

For the real-time scope, the aggressor jitter histogram is Gaussian-like to approximately ± 5 standard deviations due to its great length and the pseudo-random nature. This Gaussian-like histogram extends to a very low BER (as low as 10^{-9}), which is lower than the scope is capable of measuring. Therefore, the aggressor effectively masked RJ

behavior in the Q-scale. Consequently, the PRBS $2^{31}-1$ aggressor corrupted RJ in the real-time scope as well.

For both scopes, the DDJ was uncorrupted because the aggressor was not correlated to the victim. For the sampling scope, the aggressor corrupted the uncorrelated jitter, but the excess jitter was accounted for by the corrupted RJ, leaving PJ unaffected. For the real-time scope, the jitter spectrum could not resolve the aggressor lines, also leaving PJ unaffected.

These three examples show that by simply varying the aggressors' data pattern, crosstalk can induce false readings of RJ, PJ, or DDJ in common jitter analyzers. The coupling mechanism was simply the deliberate sharing of a power supply between transmit buffers and their clocking PLL.

Correlation With Laboratory Simulation

We reproduced the behavior of crosstalk affecting a victim's jitter in the laboratory using common, off-the-shelf equipment. We show a correlation in trend with the effects seen in the degraded transceiver test chip in Section 0. Figure 19 shows the schematic for the setup consisting of an Agilent 81134 pattern generator and an oscilloscope for jitter measurement.

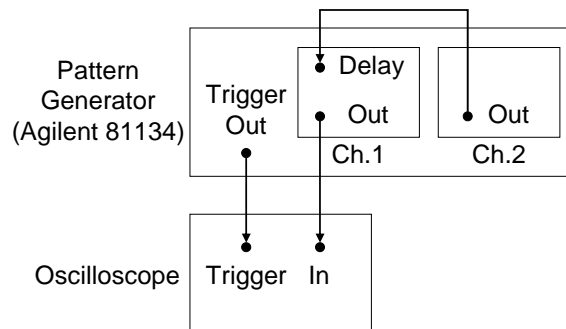


Figure 19: Schematic for laboratory simulation of crosstalk affecting jitter.

The pattern generator was configured to transmit data at 2.5 Gbps from both channels. Channel 1 served as the victim and transmits a PRBS $2^{10}-1$. Channel 2 served as the aggressor and transmitted various data patterns. The output of Channel 2 was applied to the time delay input of Channel 1. The time delay function converted a voltage signal to a proportional delay in the timing of the signal. The conversion scale of the time delay was 25 ps/volt and is band-limited to 200 MHz. Effectively, this allowed the filtered voltage output of Channel 2 to modulate the timing of Channel 1. While this is not representative of the inductive or capacitive coupling that we expect in a real device, it is sufficient to show behavior similar to the degraded test chip in Section 0. The output amplitude of Channel 1 was 800mV and Channel 2 was 250mV. As with the transceiver test chip, the victim's jitter was measured with both a sampling scope and a real-time scope.

Baseline

With the aggressor disabled, we measured the jitter output of the victim. The results are shown in Table 5. The most significant difference between Table 5 and Table 1 is in RJ, which is expected as the metrology-quality pattern generator is known to have a clean output.

Jitter	Sampling Scope	Real-Time Scope
RJ	1.61 ps	2.03 ps
PJ	11.5 ps ($\bar{\delta}$ - $\bar{\delta}$)	0 ps (pk-pk)
DDJ	7 ps	12 ps
TJ	39.8 ps	40.57 ps

Table 5: Comparison of jitter values for baseline measurement.

We configured the aggressor channel to transmit PRBS 2^7-1 . Table 6 shows the results. PJ was increased by approximately 15 to 17 ps, which is comparable to the 12 to 15 ps increase observed in the transceiver test chip (Table 2). RJ and DDJ remain unchanged, as expected. TJ was proportionally affected.

Jitter	Sampling Scope	Real-Time Scope
RJ	1.87 ps	2.39 ps
PJ	28.8 ps ($\bar{\delta}$ - $\bar{\delta}$)	15.3 ps (pk-pk)
DDJ	7.5 ps	13.3 ps
TJ	60.8 ps	62.3 ps

Table 6: Comparison of jitter values for PRBS 2^7-1 aggressor pattern.

We configured the aggressor channel to transmit PRBS $2^{10}-1$. Table 7 shows the results. DDJ was impacted, increasing by nearly 20 ps. This increase is similar to the 15 to 18 ps increase seen in the transceiver test chip (Table 3). The RJ and DJ values were relatively unaffected.

Jitter	Sampling Scope	Real-Time Scope
RJ	1.66 ps	1.71 ps
PJ	11.4 ps ($\bar{\delta}$ - $\bar{\delta}$)	0 ps (pk-pk)
DDJ	28.1 ps	31.9 ps
TJ	58.4 ps	55.9 ps

Table 7: Comparison of jitter values for PRBS $2^{10}-1$ aggressor pattern.

For the aggressor channel configured to PRBS $2^{31}-1$, the results are shown in Table 8. The RJ values were severely affected. The trend is consistent with the transceiver test chip (Table 4), but the specific values are different due to different RJ baselines. PJ and DDJ were unaffected. TJ was affected disproportionately as expected.

Jitter	Sampling Scope	Real-Time Scope
RJ	6.4 ps	3.4 ps
PJ	2.2 ps ($\bar{\delta}$ - $\bar{\delta}$)	0 ps (pk-pk)
DDJ	7.4 ps	13.1 ps
TJ	90.1 ps	60.8 ps

Table 8: Comparison of jitter values for PRBS $2^{31}-1$ aggressor pattern.

These simple laboratory experiments effectively reproduced the same phenomena observed in the degraded transceiver test chip. By varying the aggressor data pattern, we were able to observe the expected impact on the victim's jitter. In some cases, we were able to reproduce the similar increases in specific jitter values. These laboratory experiments correlate well with the behavior observed on the transceiver test chip.

Summary and Conclusions

The importance of understanding the effects of crosstalk on jitter increases perpetually. Often, crosstalk-related jitter is marginally addressed in most jitter analysis. We presented real-life situations where crosstalk resulted in significant increases in the victim's jitter. Furthermore, a simple manipulation of the aggressors' data pattern caused the crosstalk's effects to appear as PJ, DDJ, or RJ. As a result, TJ is also affected. In the case of increased RJ, TJ is further inflated due to the conversion from rms to peak-to-peak values.

The basis for this knowledge lies in the understanding of spectra of various waveforms. It is equally important to understand how these spectra can be misinterpreted by common jitter analysis methodologies. Familiarity with these techniques allows engineers to diagnose and debug crosstalk-related issues in their applications.

References

- [1] R. Stephens, A. Neves, "Characterizing, Anticipating, and Avoiding Problems with Crosstalk," Proceedings of DesignCon, 2006.
- [2] M. Li, "Recent Developments in Jitter and Signal Integrity Measurement and Analysis at Multiple Gb/s or GHz," Proceedings of DesignCon, 2007.
- [3] A., Kuo, et al., "Crosstalk Bounded Uncorrelated Jitter (BUJ) for High-Speed Interconnects," IEEE Transactions on Instrumentation and Measurement, Vol. 54, Issue 5, 2005.
- [4] A., Kuo, et al., "Jitter Models and Measurement Methods for High-Speed Serial Interconnects," 1st Annual TTTC Gigabit Test Workshop, 2004.
- [5] Federal Standard 1037C, "Glossary of Telecommunication Terms," 2000.
- [6] "Synchronization Interface Standards for Digital Networks," ANSI T1.101-1987.
- [7] For Fourier transform of an exponential function, please refer to <http://mathworld.wolfram.com/FourierTransformExponentialFunction.html>.
- [8] "Fibre Channel Methodologies for Jitter and Signal Quality Specification (MJSQ)," www.t11.org/ftp/t11/pub/fc/mjsq/04-101v5.pdf.



101 Innovation Drive
San Jose, CA 95134
www.altera.com

Copyright © 2008 Altera Corporation. All rights reserved. Altera, The Programmable Solutions Company, the stylized Altera logo, specific device designations, and all other words and logos that are identified as trademarks and/or service marks are, unless noted otherwise, the trademarks and service marks of Altera Corporation in the U.S. and other countries. All other product or service names are the property of their respective holders. Altera products are protected under numerous U.S. and foreign patents and pending applications, maskwork rights, and copyrights. Altera warrants performance of its semiconductor products to current specifications in accordance with Altera's standard warranty, but reserves the right to make changes to any products and services at any time without notice. Altera assumes no responsibility or liability arising out of the application or use of any information, product, or service described herein except as expressly agreed to in writing by Altera Corporation. Altera customers are advised to obtain the latest version of device specifications before relying on any published information and before placing orders for products or services.